



HAL
open science

Cosmogenic effects on Cu isotopes in IVB iron meteorites

Heng Chen, Frédéric Moynier, Munir Humayun, M. Cole Bishop, Jeffrey Williams

► **To cite this version:**

Heng Chen, Frédéric Moynier, Munir Humayun, M. Cole Bishop, Jeffrey Williams. Cosmogenic effects on Cu isotopes in IVB iron meteorites. *Geochimica et Cosmochimica Acta*, 2016, 182, pp.145-154. 10.1016/j.gca.2016.03.006 . insu-02917560

HAL Id: insu-02917560

<https://insu.hal.science/insu-02917560>

Submitted on 20 Aug 2020

HAL is a multi-disciplinary open access archive for the deposit and dissemination of scientific research documents, whether they are published or not. The documents may come from teaching and research institutions in France or abroad, or from public or private research centers.

L'archive ouverte pluridisciplinaire **HAL**, est destinée au dépôt et à la diffusion de documents scientifiques de niveau recherche, publiés ou non, émanant des établissements d'enseignement et de recherche français ou étrangers, des laboratoires publics ou privés.

Cosmogenic Effects on Cu Isotopes in IVB Iron Meteorites

Heng Chen^{a*}, Frédéric Moynier^{a,b,c}, Munir Humayun^d, Matthew C. Bishop^a, Jeffrey T. Williams^{d,e}

^a Department of Earth and Planetary Sciences and McDonnell Center for the Space Sciences, Washington University in St. Louis, One Brookings Drive, St. Louis, MO 63130, USA

^b Institut de Physique du Globe de Paris, Université Paris Diderot, Sorbonne Paris Cité, CNRS, 1 Rue Jussieu, Paris 75238, France

^c Institut Universitaire de France, Paris, 75005, France

^d National High Magnetic Field Laboratory and Department of Earth, Ocean & Atmospheric Science, Florida State University, Tallahassee, FL 32310, USA.

^e Presently at: Department of Earth and Planetary Sciences, University of New Mexico, Albuquerque, NM 87131, USA.

*Corresponding author

Email address: chenheng@levee.wustl.edu

Tel: +1 314 660 9748

1 **Abstract**

2 We measured Cu isotope compositions of 12 out of the 14 known IVB iron meteorites. Our results show
3 that IVB iron meteorites display a very large range of $\delta^{65}\text{Cu}$ values ($-5.84\text{‰} < \delta^{65}\text{Cu} < -0.24\text{‰}$; defined
4 as per mil deviation of the $^{65}\text{Cu}/^{63}\text{Cu}$ ratio from the NIST-976 standard). These Cu isotopic data display
5 clear correlations with W, Pt, and Os isotope ratios, which are very sensitive to secondary neutron capture
6 due to galactic cosmic ray (GCR) irradiation. This demonstrates that $\delta^{65}\text{Cu}$ in IVB irons is majorly
7 modified by neutron capture by the reaction $^{62}\text{Ni}(n,\gamma)^{63}\text{Ni}$ followed by beta decay to ^{63}Cu . Using
8 correlations with Pt and Os neutron dosimeters, we calculated a pre-exposure $\delta^{65}\text{Cu}$ of $-0.3 \pm 0.8\text{‰}$ (95%
9 conf.) of IVB irons that agrees well with the Cu isotopic compositions of other iron meteorite groups and
10 falls within the range of chondrites. This shows that the volatile depletion of the IVB parent body is not
11 due to evaporation that should have enriched IVB irons in the heavy Cu isotopes.

12

13 **Keywords:** IVB iron meteorites; Copper isotopes; Cosmic ray exposure; Neutron capture

14 1. Introduction

15 Copper is a moderately volatile element ($T_c=1037$ K; Lodders, 2003), and follows a chalcophile
16 /siderophile behavior during planetary differentiation processes (Righter et al., 2010). It has two stable
17 isotopes: ^{63}Cu (69.17%) and ^{65}Cu (30.83%) and even though few data have been published on the natural
18 fractionation of Cu isotopes in terrestrial rocks, it seems that Cu has a very limited isotopic fractionation
19 during igneous processes (Savage et al., 2015). In a survey of the Cu isotope compositions of iron
20 meteorites, Bishop et al. (2012) observed that IVB irons ($n=3$) had distinctly negative $\delta^{65}\text{Cu}$ ($\sim -2\%$;
21 $\delta^{65}\text{Cu}$ defined as the per mille deviation of a sample's $^{65}\text{Cu}/^{63}\text{Cu}$ compositional ratio from that of the
22 NIST-976 standard), which deviates from the values of chondrites ($-1.51\text{‰} < \delta^{65}\text{Cu} < 0.07\text{‰}$; Luck et
23 al., 2003; Barrat et al., 2012) and other iron meteorite groups ($-1.83\text{‰} < \delta^{65}\text{Cu} < 0.99\text{‰}$; Luck et al.,
24 2005; Bishop et al., 2012). Magmatic iron meteorites are believed to represent samples of the metallic
25 cores of small planetary bodies (Scott, 1972). Among iron meteorite groups, the IVB group is the most
26 volatile depleted with low concentrations of moderately volatile elements (*e.g.* Ga, Ge, and Cu) coupled
27 with high concentrations of Ni (16 – 18 wt.%) and other refractory elements (*e.g.* Ir, Re; Campbell and
28 Humayun, 2005; Walker et al., 2008). **Bishop et al. (2012) proposed a precursor with a non-chondritic Cu
29 isotopic composition for the IVB parent body to explain their uniquely light Cu isotopic composition.
30 This explanation contradicts the prediction that angrites may represent the silicate portion of the IVB
31 parent body (Campbell and Humayun, 2005).**

32 The $^{182}\text{Hf}-^{182}\text{W}$ system ($t_{1/2} = 8.9 \pm 0.1$ Myr; Vockenhuber et al., 2004) has proven to be a very
33 important short-lived chronometer for dating metal-silicate differentiation events that occurred in the first
34 60 Myrs of the Solar System's history (Kleine et al., 2002; Schoenberg et al., 2002; Yin et al., 2002;
35 Kleine et al., 2004; Jacobsen, 2005; Moynier et al., 2010a). **However, some of the iron meteorites were
36 found to have lower $\epsilon^{182}\text{W}$ values (relative deviation of the ratio of ^{182}W to a stable W isotope from a
37 terrestrial standard in parts per 10^4 ; Kleine et al., 2005; Lee, 2005; Markowski et al., 2006a; Schersten et
38 al., 2006; Qin et al., 2008) than the initial $\epsilon^{182}\text{W}$ value (-3.51 ± 0.10) of the calcium-aluminum-rich**

39 inclusions (CAIs; Burkhardt et al., 2012). The abnormally low $\epsilon^{182}\text{W}$ values in these iron meteorites
40 reflect superimposed neutron capture effects that result from long-duration exposure to galactic cosmic
41 rays (GCR; Masarik, 1997; Leya et al., 2003; Markowski et al., 2006a, 2006b; Qin et al., 2008). When
42 subjected to intense GCR irradiation, particles with energies of several MeV or more may induce nuclear
43 reactions, including spallation and secondary neutron capture reactions in meteorites. Most iron
44 meteorites have cosmic-ray exposure ages of several hundred Myrs, much larger than stony meteorites
45 (Voshage and Feldmann, 1979; Voshage, 1984). Recent studies have found that neutron capture effects
46 also modify the isotopic compositions of some other siderophile elements (e.g., Os, Ir, Pt, Rh, Pd) in iron
47 meteorites (Walker, 2012; Wittig et al., 2013; Kruijer et al., 2013; Kruijer et al., 2014; Mayer et al., 2015);
48 for example, neutron capture reactions create detectable ^{192}Pt and ^{190}Os excesses coupled with ^{189}Os
49 deficits (Walker, 2012; Wittig et al., 2013; Kruijer et al., 2013; Kruijer et al., 2014). These siderophile
50 elements have comparable cross sections for secondary neutrons to W, so cosmogenic Pt and Os isotopic
51 anomalies have been applied as *in situ* neutron dosimeters for ^{182}W correction (Kruijer et al., 2013; Wittig
52 et al., 2013; Kruijer et al., 2014).

53 Among all the Ni isotopes, ^{62}Ni has the largest thermal neutron capture cross section (14.5 barns) and
54 epithermal resonance integral (6.6 barns; Mughabghab, 2003), so a potential neutron capture reaction,
55 $^{62}\text{Ni}(n,\gamma)^{63}\text{Ni}(\beta^-)^{63}\text{Cu}$ might have produced excessive ^{63}Cu in these IVB irons due to extremely high Ni/Cu
56 ratio ($\sim 1.1 \times 10^5$; 3 orders of magnitude higher than the ratios in CI chondrites), leading to some very low
57 $\delta^{65}\text{Cu}$ values as observed by Bishop et al. (2012). Thus, studying Cu isotopic variations among IVB irons
58 is essential to constrain the magnitude of cosmogenic neutron capture to Cu isotopes.

59 In the present study, we measured Cu isotope compositions of 12 IVB iron meteorites from the same
60 samples analyzed for W, Os, and Pt isotope compositions (Wittig et al., 2013) and found a good
61 correlation between Cu isotopes and recently published W, Os, and Pt data, which are known to be
62 modified by GCR neutron capture processes. We suggest that the Cu isotopic compositions of IVB
63 meteorites are controlled by neutron capture effects on ^{62}Ni . We further correct for the neutron capture

64 effect on Cu isotopes by coupling our data with previously measured Pt and Os isotopes to obtain a pre-
65 irradiation value of $\delta^{65}\text{Cu}$ for IVB irons.

66

67 **2. Samples**

68 In order to test our assumption that Cu isotopes of IVB iron meteorites have been modified by GCR,
69 the Cu isotopic compositions of 12 of the 14 known IVB iron meteorites were measured by high-
70 precision Multiple-Collector Inductively Coupled Plasma Mass Spectrometry (MC-ICP-MS). Since
71 neutron capture effects vary with depth within a meteorite body, these samples were taken within 2 mm
72 from the samples for which Pd, Os, Pt, and W isotopic compositions have been reported by Wittig et al.
73 (2013) and Mayer et al. (2015). This sample set, based on previously reported cosmic ray exposure age
74 data (Voshage and Feldmann, 1979) and W isotope compositions (Kleine et al., 2005; Markowski et al.,
75 2006a; Qin et al., 2008; Wittig et al., 2013; Kruijer et al., 2013, 2014) is likely to cover a wide range in
76 degrees of GCR irradiation.

77 In addition, we also report Cu isotopic compositions of 7 USGS geostandards (dunite DTS-1,
78 peridotite PCC-1, andesite AGV-2, and basalts BCR-1, BCR-2, BIR-1, and BHVO-2) in order to test the
79 reproducibility of our analytical technique, as well as to provide more data on the Cu isotopic
80 composition of the Earth.

81

82 **3. Analytical methods**

83 Based on estimated Cu concentrations, 0.5 – 1 g of metal was cut and polished for isotopic analysis.
84 Metallic chips were first cleaned in diluted HCl, and then rinsed with deionized water in an ultrasonic
85 bath to get rid of surface contamination. Cleaned samples were digested in aqua regia in PTFE containers
86 under hot lamps for > 48 hours until complete dissolution was observed. Purification of Cu was achieved

87 by anion exchange chromatography following the procedure described in Marechal et al. (1999) and
88 Bishop et al. (2012). The samples were loaded in 1 ml of 7 mol/L HCl on 1.6 mL of anion-exchange resin
89 (AGMP1). Matrix elements were eluted by 7 ml of 7 mol/L HCl and Cu was extracted by further addition
90 of 19 ml of 7 mol/L HCl. This process was repeated twice to further purify Cu.

91 Copper isotopic compositions were measured on a Thermo-Finnigan Neptune Plus™ MC-ICP-MS at
92 Washington University in St. Louis following the procedure described in Weinstein et al. (2011) and
93 Bishop et al. (2012). Samples were introduced into the mass spectrometer in 0.1 mol/L HNO₃ via a CPI™
94 PFA nebulizer attached to a glass spray chamber. All samples and standards were adjusted to the same
95 concentration (150 ± 10 ppm) for mass spectrometer analysis. Isotope intensities were collected
96 simultaneously in static mode using a multiple faraday collector array. Twenty-five integrations of 5 s
97 duration were acquired during one sample measurement with an associated internal error on the ⁶⁵Cu/⁶³Cu
98 of about 2-4 × 10⁻⁶.

99 Isotope measurements were performed using standard-sample bracketing to correct for any instrumental
100 drift over time. Copper isotopic ratio is expressed in δ per mil units with respect to the standard NIST-976
101 as:

$$102 \quad \delta^{65}\text{Cu} = [({}^{65}\text{Cu} / {}^{63}\text{Cu}_{\text{sample}}) / ({}^{65}\text{Cu} / {}^{63}\text{Cu}_{\text{NIST-976}}) - 1] \times 1000$$

103 Each sample was measured at least twice and the average is reported. The blank of the total procedure
104 (dissolution and chemical purification) is < 5 ng, which is negligible compared with the total amount of
105 Cu present in the samples (> 300 ng). The external reproducibility (2 s.d.) of the δ⁶⁵Cu is 0.10 ‰ for iron
106 meteorites (see Bishop et al., 2012).

107 The Ni and Cu concentrations were determined by laser ablation ICP-MS at Florida State University
108 following the method described in Humayun (2012) and Williams and Humayun (2013).

109

110 **4. Results**

111 The Cu isotopic compositions of well-characterized USGS standards (DTS-1, PCC-1, AGV-2, BCR-1,
112 BCR-2, BIR-1, and BHVO-2) are listed in Table 1 together with some previously reported analyses. The
113 good agreement between our data and literature values demonstrates the robustness of the methods and of
114 our analyses. These igneous geostandard samples have very similar Cu isotopic compositions within the
115 errors, showing a typical terrestrial composition, which scatters around 0 ‰ (Albarède, 2004; Ben
116 Othman et al., 2006).

117 The Ni and Cu concentration and Cu isotopic composition for each of the 12 IVB iron meteorites are
118 listed in Table 2, together with corresponding W, Pt, and Os isotope data from Wittig et al. (2013). The
119 IVB irons display relatively small variations in Ni (15.68 – 17.87 wt.%) and Cu (1.26 – 1.79 ppm)
120 contents, with Ni/Cu ratio ranging from $9.9 - 12.9 \times 10^4$, $\sim 10^2$ higher than in IVA iron meteorites.

121 Although a small nucleosynthetic anomaly in $\epsilon^{184}\text{W}$ has been confirmed in IVB irons, the nucleosynthetic
122 anomalies are negligible on $\epsilon^{182}\text{W}$ (Qin et al., 2008; Wittig et al., 2013; Kruijer et al., 2013). The $\delta^{65}\text{Cu}$
123 values of IVB irons are widely scattered between -0.24 and -5.84 ‰. Compared with chondrites and other
124 groups of iron meteorites, IVB irons have a much larger $\delta^{65}\text{Cu}$ span, and most of them display significant
125 enrichment in ^{63}Cu isotopes (or depletion in ^{65}Cu). Of the IVB iron meteorites, Weaver Mountains is the
126 least modified by GCR-induced ^{182}W burn-out and has the highest $\delta^{65}\text{Cu}$ value, falling within the range of
127 chondrites and other iron meteorites. In contrast, Tlacotepec, one of the most cosmic ray-irradiated
128 samples, has the lowest $\delta^{65}\text{Cu}$ measured in this study, of -5.84 ‰, which deviates the most from the
129 average composition of chondrites.

130

131 **5. Discussion**

132 *5.1 Mechanisms of Cu isotopic fractionation*

133 Compared with chondrites and terrestrial igneous rocks, iron meteorites as a whole display larger Cu
134 isotopic fractionation, however, Cu isotopic compositions among most individual iron groups are

135 relatively homogeneous ($\leq 1\%$). The IVB iron meteorites show a much larger range of variability ($\sim 6\%$),
136 and the IVB is the only group that does not fall within the chondritic range. It was suggested that mass-
137 dependent processes such as evaporation-condensation and fractional crystallization could account for the
138 small variations within the group (Bishop et al., 2012), but it is unclear that such processes could
139 fractionate Cu isotopes to the magnitude observed in the IVB group. In the following sections we will
140 consider the different possible mechanisms of Cu isotopic fractionation.

141 *5.1.1 Copper isotope fractionation during low-temperature alteration processes*

142 Low-temperature alteration and biological processes could generate significant Cu isotopic fractionations
143 (Albarède, 2004). For example, iron and copper minerals from supergene profile of the Bayugo porphyry
144 copper-gold deposit yielded $\delta^{65}\text{Cu}$ values between -3.4 and $+6.9\%$ (Braxton and Mathur, 2011).
145 However, any low-temperature fractionation process (*e.g.* aqueous alteration) that occurred on the IVB
146 parent body prior to the core formation would have been homogenized in the melt from which all IVB
147 irons crystallized, and would not be expected to create large isotopic variations among individual IVB
148 irons. Previous studies on Re–Os isotopic systematics (Walker et al., 2008) and siderophile element
149 concentrations in IVB irons (Campbell and Humayun, 2005; Walker et al., 2008) both confirmed that
150 their parent body remained a chemically closed system after crystallization. In addition, our samples were
151 specifically selected from polished interior slices, free from fusion crust or from oxidation products. Each
152 sample was polished to remove sawn surfaces. Therefore, Cu isotopic variations in these samples should
153 not be the result of alteration that occurred after crystallization either.

154 *5.1.2 Copper isotope fractionation during evaporation processes*

155 Copper is a moderately volatile element, with a 50 % condensation temperature (T_c) of 1037 K (Lodders,
156 2003). Previous studies have observed that Cu isotopes are substantially fractionated during evaporation-
157 condensation processes (Herzog et al., 2009; Moynier et al., 2010b). The IVB group contains the lowest
158 concentrations of moderately volatile elements among all iron meteorite groups, which either reflects high
159 nebular temperatures when their parent body accreted or volatile loss during one or more impacts

160 (Rasmussen et al., 1984; Campbell and Humayun, 2005). During the process of evaporation, light
161 isotopes of an element are preferentially lost into vapor, leaving the residual phase enriched in heavier
162 isotopes (Humayun and Clayton, 1995; Humayun and Cassen, 2000). This has been observed in shock-
163 melted rocks (Albarede et al., 2004), especially in the tektites (hypervelocity impact glasses) that are
164 among the terrestrial samples with the heaviest Cu isotopic composition ($\delta^{65}\text{Cu}$ up to 6.99 ‰; Moynier et
165 al., 2010b), although no such fractionation of potassium ($T_c = 1006 \text{ K}$) isotopes is observed in tektites or
166 in impact melts (Humayun and Clayton, 1995; Humayun and Koeberl, 2004). Since IVB irons are
167 significantly depleted in heavier Cu isotopes, which is opposite to what is expected from an evaporation
168 process (Fig. 1), our new data agree with the conclusions by Bishop et al. (2012) that partial vaporization
169 did not modify Cu isotopes in IVB irons, and that the severe depletions of Cu and other moderately
170 volatile elements in IVB irons must have been induced by other mechanisms.

171 *5.1.3 Copper isotope fractionation during igneous processes*

172 Although the volatile history and accretion processes of IVB parent body are still under debate (Campbell
173 and Humayun, 2005; Walker et al., 2008; Yang et al., 2010; Williams and Humayun, 2013), the variations
174 of chemical compositions within the IVB group can be successfully modeled as the result of simple
175 crystallization of the metallic liquid in a closed system (Walker et al., 2008). Previous studies have
176 suggested that isotopic fractionations observed in iron meteorites might have been created during the
177 partitioning of Cu between metal and silicates (Luck et al., 2003; Moynier et al., 2007). **Metal-silicate**
178 **fractionation could give rise to a small isotope shift of the parental IVB metallic liquid relative to any**
179 **plausible chondritic starting composition, and Savage et al. (2015) showed that this was < 0.1‰.** The
180 magmatic differentiation is unlikely to account for the Cu isotopic variations observed in IVB irons for
181 the following reasons:

182 First, no such large span of $\delta^{65}\text{Cu}$ has been found in any other group of magmatic iron meteorites, which
183 exhibits similar or even larger ranges of fractional crystallization (Goldstein et al., 2009). Current studies
184 have shown that most of the iron groups have relatively homogeneous Cu isotopic composition ($\delta^{65}\text{Cu}$

185 variation < 1 ‰) within each group (Bishop et al., 2012). Among all the major iron meteorite systems,
186 IVB group has the simplest chemical evolution that resulted from crystallization of a metallic liquid
187 (Walker et al., 2008), so it is unlikely that magmatic differentiation could induce $\delta^{65}\text{Cu}$ fractionation up to
188 5.6 ‰ in IVB irons.

189 Second, $\delta^{65}\text{Cu}$ variation is independent of magmatic evolution among IVB irons. Rhenium (Re) is a
190 highly compatible element, whose concentration decreases with increasing degree of fractional
191 crystallization, and thus it has been applied as an indicator of magmatic differentiation in iron meteorites
192 (Walker et al., 2008). **During fractional crystallization, Cu isotope fractionation between solid metal and
193 the residual liquid may give rise to Cu isotope differences that are a function of the extent of fractional
194 crystallization. Since Cu isotopes do not correlate with Re abundances (Fig. 2, $R^2 = 0.16$), this effect is
195 not important in controlling the Cu isotope composition of individual IVB irons.**

196 Finally, the published Cu isotopic data of igneous rocks showed that Cu isotopic fractionation induced by
197 magmatic differentiation is rather limited (Savage et al. 2015). The $\delta^{65}\text{Cu}$ values of igneous standards
198 derived from different geological settings (see table 1) and unaltered igneous rocks acquired by previous
199 studies are narrowly distributed between -0.1 and 0.3 ‰ (Albarède, 2004; Ben Othman et al., 2006; Li et
200 al., 2009; Savage et al., 2015). Although these igneous rocks went through different degrees of fractional
201 crystallization, the variations of Cu isotopes are much smaller than what was measured in IVB irons
202 (5.6 ‰). **Therefore we conclude that it is unlikely that high-temperature magmatic processes could induce
203 $\delta^{65}\text{Cu}$ fractionation up to the scale of 5.6 ‰ as observed in IVB irons.**

204 *5.1.4 Nucleosynthetic Effects and short-lived radionuclides in Iron Meteorites*

205 **Copper has only two stable isotopes, and thus it is impossible to differentiate between mass-dependent
206 and mass-independent fractionation (e.g. nucleosynthetic effect and radioactive decay). However, from
207 the discussion above, we exclude mass-dependent fractionation processes such as low-temperature
208 alteration, high-temperature volatilization, and magmatic differentiation as the major processes that
209 fractionate Cu isotopes in IVB irons. For some metal elements, mass-independent effects have been
210 observed in iron meteorites. e.g. Ni (Regelous et al. 2008), Cr (Trinquier et al. 2007), Mo (Dauphas et al.**

211 2002; Burkhardt et al., 2011), Ru (Chen et al. 2010; Fischer-Gödde et al., 2015) and Pd (Mayer et al.,
212 2015). These isotopic anomalies most likely result from heterogeneous distribution of isotopically diverse
213 presolar dust in the Solar System at the time when iron meteorite parent bodies formed (Trinquier et al.,
214 2007; Burkhardt et al., 2011). However, the magnitudes of nucleosynthetic effects in these elements are
215 rather small ($< 0.1\text{‰ amu}^{-1}$). For example, the total ranges of $\epsilon^{60}\text{Ni}_{58/61}$, $\epsilon^{62}\text{Ni}_{58/61}$, and $\epsilon^{64}\text{Ni}_{58/61}$ in iron
216 meteorites (including IC, IIAB, IIIAB, IVA, IVB) are only 0.14, 0.36, and 0.69 per ten thousand,
217 respectively (Steele et al., 2011). In addition, any nucleosynthetic anomalies should be present in all IVB
218 irons equally after the melting and differentiation of parent body. Therefore, even if Cu isotopes were not
219 well mixed in the Solar System by the time of IVB parent body formation, the magnitude of
220 nucleosynthetic effect on $\delta^{65}\text{Cu}$ is very unlikely to be more than 0.1 ‰, which is negligible compared to
221 the range of Cu isotopes in IVB irons.

222 The radioactive decay of some short-lived radionuclides, which were synthesized in stars or by irradiation
223 in the early Solar System, could also create isotopic anomalies in meteorites and their components (e.g.
224 Lee et al., 1976; Lugmair and Shukolyukov, 1998). The decay of the short-lived nuclide ^{63}Ni produces
225 ^{63}Cu by beta decay. The presence of ^{63}Ni at the time of fractional crystallization in the IVB iron parent
226 body could potentially lead to variation of $\delta^{65}\text{Cu}$ among individual irons, which is due to different
227 parent/daughter ($^{63}\text{Ni}/^{63}\text{Cu}$) ratios created by chemical differentiation.

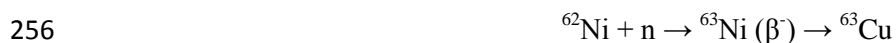
228 After melting and mixing inside the IVB parent body, the short-lived ^{63}Ni is expected to be
229 homogeneously distributed throughout the melt from which all IVB irons crystallized. The radiogenic
230 ingrowth model is shown in Figure 3, assuming a $^{63}\text{Ni}/^{60}\text{Ni}$ of 1×10^{-5} at the birth of the Solar System and a
231 $\delta^{65}\text{Cu}$ of 0 at the time of fractional crystallization. All the variations of $\delta^{65}\text{Cu}$ and Ni/Cu reflect the growth
232 with time of radiogenic ^{63}Cu excesses due to decay of short lived ^{63}Ni . The four isochron lines (with a
233 solidification age of 500, 750, 1000, 1250, and 2000 years respectively) display linearly negative
234 correlation between $\delta^{65}\text{Cu}$ and the Ni/Cu ratio. Had the IVB irons crystallized very quickly after the birth
235 of the Solar System (e.g. < 1000 years after the synthesis of ^{63}Ni nuclide), resolvable $\delta^{65}\text{Cu}$ differences

236 could be detected between individual IVB irons due to different Ni/Cu ratios. However, as the half-life of
237 ^{63}Ni is only 100.1 years, which is thousand times shorter than the shortest known isotope chronometers
238 found in meteorites, *e.g.*, ^{41}Ca (1.02×10^5 years), ^{26}Al (7.17×10^5 years), etc., it is too short-lived to have
239 been present in the early Solar System. Even though we used a higher initial $^{63}\text{Ni}/^{60}\text{Ni}$ ratio (1×10^{-5}) than
240 the estimation ($\sim 5 \times 10^{-6}$) by Luck et al. (2003), as the model predicted, no resolvable $\delta^{65}\text{Cu}$ fractionation
241 due to the radioactive decay of ^{63}Ni would exist if fractional crystallization occurred 2000 years after the
242 production of ^{63}Ni nuclides. The IVB irons formed about ~ 1 Ma after CAIs (Wittig et al., 2013; Kruijer et
243 al., 2013), so it is inconceivable that nucleosynthetic ^{63}Ni could have been present in the parental liquid
244 from which IVBs formed.

245 If ^{63}Ni was present at the time of crystallization of the IVB iron meteorites, a linear anti-correlation
246 between the Ni/Cu ratio of individual irons and their $\delta^{65}\text{Cu}$ would be expected. However, there is no clear
247 correlation between $\delta^{65}\text{Cu}$ and Ni/Cu ratio observed in the IVB irons (Fig. 3), therefore, the $\delta^{65}\text{Cu}$
248 variation is unlikely the result of radioactive decay of nucleosynthetic ^{63}Ni .

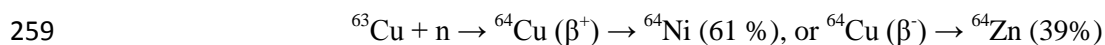
249 5.2 Neutron capture effects on Cu isotopes during GCR-exposure

250 IVB iron meteorites have large GCR exposure ages of 200-950 Myrs (Voshage and Feldmann, 1979;
251 Herzog, 2007). When exposed to GCR irradiation, secondary neutrons produced by cosmic ray spallation
252 in iron meteorites are captured by siderophile element nuclei. These neutrons are dominantly captured by
253 the most abundant nuclides in iron meteorites, including Fe, Ni, and Co (Leya and Masarik, 2013).
254 Among the Ni isotopes, ^{62}Ni has a thermal neutron capture cross section an order of magnitude larger than
255 for other Ni isotopes or for Fe isotopes (Mughabghab, 2003). For ^{62}Ni , there is the following reaction:



257 ^{62}Ni captures a neutron to produce ^{63}Ni ; since ^{63}Ni ($t_{1/2}$: 100.1 y) is unstable, it quickly decays to ^{63}Cu .

258 Similarly, for Cu isotopes (note the branching beta decay):



260 Although both ^{63}Cu and ^{65}Cu can also be burned out by capturing secondary neutrons, the direct effect is
261 negligible compared to the production of cosmogenic ^{63}Cu from ^{62}Ni , because ^{63}Cu and ^{65}Cu have smaller
262 neutron capture cross sections (4.5 and 2.2 barns, respectively) than ^{62}Ni , and the $^{62}\text{Ni}/^{63}\text{Cu}$ ratio is as high
263 as 5×10^3 in IVB irons. Given the long exposure to GCR, the accumulated ^{63}Cu from ^{62}Ni burn-out leads to
264 a resolvable decrease in $^{65}\text{Cu}/^{63}\text{Cu}$ value in IVB iron meteorites. It should be pointed out that the total
265 burn-out on ^{62}Ni is too small ($<0.001\%$; calculated from $\delta^{65}\text{Cu}$ deviation) to be detected by measuring Ni
266 isotopic ratios under current analytical precisions ($\sim 0.05\%$; Moynier et al. 2007; Regelous et al. 2008),
267 even in the most irradiated sample, Tlacotepec. Similarly, variations in $\delta^{65}\text{Cu}$ are not affected measurably
268 by direct GCR burning of the Cu isotopes.

269 The deviation of $\delta^{65}\text{Cu}$ from its pre-exposure value depends on the Ni/Cu ratio and the dosage of
270 secondary neutrons. The higher the Ni/Cu ratio and longer the galactic cosmic ray exposure is, the larger
271 the deviation from the pre-exposure value would be. In IVB iron meteorites, $\delta^{65}\text{Cu}$ values display an
272 apparent positive correlation with $\epsilon^{189}\text{Os}$ and negative correlations with $\epsilon^{190}\text{Os}$ and $\epsilon^{192}\text{Pt}$ that were
273 measured on a sample taken within 2 mm from our samples (Fig. 4), with Weaver Mountain and
274 Tlacotepec representing the least and most irradiated samples. This implies that $\delta^{65}\text{Cu}$ of IVB irons was
275 modified by neutron capture effects.

276 The IVB irons contain exceptionally low concentrations of moderately volatile elements (*e.g.* Ga, Ge, and
277 Cu) and high Ni contents (16 – 18 wt.%). The Cu concentrations of IVB irons measured in this study are
278 1.26-1.77 ppm (Table 2), while most of samples from other groups studied by Bishop et al. (2012) have
279 Cu concentrations higher than 100 ppm. The Ni/Cu ratios of IVB group members are generally ~ 100
280 times higher than in other groups of iron meteorites, indicating the deviations of $\delta^{65}\text{Cu}$ induced by GCR
281 irradiation for IVB irons are expected to be 2 orders of magnitude larger than in other iron meteorite
282 groups, given the same cosmic-ray exposure history. For example, given the $\delta^{65}\text{Cu}$ difference (5.6‰)
283 between the most (Tlacotepec) and the least cosmic ray damaged sample (Weaver Mountains) in IVB
284 group, it is possible to estimate from the Ni/Cu ratios that for other iron meteorites with equally long

285 exposure-ages as Tlacotepec (945 ± 55 ma; Voshage and Feldmann, 1979), the $\delta^{65}\text{Cu}$ shift induced by
286 neutron capture effects on ^{62}Ni is expected to be no more than 0.1 ‰, which is barely beyond our current
287 analytical uncertainties. This explains why significantly negative $\delta^{65}\text{Cu}$ only appears in the IVB group
288 and why Cu isotope variations of other iron meteorite groups (except IVBs) are close to the range defined
289 by chondrites. However, several volatile-depleted ungrouped irons with long exposure ages, e.g., Deep
290 Springs (Scott, 1978; Qin et al. 2008) might also exhibit large $\delta^{65}\text{Cu}$ deviations. Neutron capture reactions
291 will need to be considered for other irons in the future.

292 5.3 Pre-exposure $\delta^{65}\text{Cu}$ value derived from correlated Cu–Os–Pt isotope systematics

293 The pre-exposure $\delta^{65}\text{Cu}$ can be obtained from the linear correlation between Cu and Pt, as well as Os
294 isotopes. As cosmogenic $\epsilon^{192}\text{Pt}$ anomalies are dependent on Ir/Pt ratios, which display a relatively large
295 variation in the IVB group (0.46-1.00 with an average of 0.74; Walker et al., 2008), it is necessary to
296 eliminate the $\epsilon^{192}\text{Pt}$ bias from chemical differences (Kruijer et al., 2013; Wittig et al., 2013). In $\delta^{65}\text{Cu}$ vs.
297 $\epsilon^{192}\text{Pt}$ space (Fig. 4c), all $\epsilon^{192}\text{Pt}$ values were normalized to a common Ir/Pt value (average value 0.74)
298 based on the neutron capture reaction. Like $\epsilon^{192}\text{Pt}$, $\delta^{65}\text{Cu}$ deviation induced by GCR also depends on
299 chemical composition (Ni/Cu ratios) and, therefore, should also be normalized to a common Ni/Cu value.
300 But due to the relatively limited Ni/Cu variations in IVB irons and possibly larger uncertainties arising
301 from a pre-exposure $\delta^{65}\text{Cu}$ assumption for normalization, $\delta^{65}\text{Cu}$ is not normalized in this study. In contrast,
302 $\epsilon^{189}\text{Os}$ and $\epsilon^{190}\text{Os}$ show anti-correlation (Wittig et al., 2013), with little dependence on the chemical
303 composition, therefore, no normalizations are needed.

304 In each systematics (Fig. 4), the dashed line is the best-fit regression to the correlation, calculated using
305 Isoplot (Ludwig, 2003). The intercepts to the pre-exposure $\epsilon^{189}\text{Os}$, $\epsilon^{190}\text{Os}$, and $\epsilon^{192}\text{Pt}$ values (by definition
306 0) represent the pre-exposure $\delta^{65}\text{Cu}$ value. The $\delta^{65}\text{Cu}$ vs. $\epsilon^{189}\text{Os}$ (Fig. 4A), $\delta^{65}\text{Cu}$ vs. $\epsilon^{190}\text{Os}$ (Fig. 4B), and
307 $\delta^{65}\text{Cu}$ vs. $\epsilon^{192}\text{Pt}$ (Fig. 4C) correlations yield pre-exposure $\delta^{65}\text{Cu}$ values of -0.3 ± 1.8 (95% conf.), $-0.5 \pm$
308 1.2 (95% conf.), -0.1 ± 1.2 (95% conf.), respectively. Since the $\epsilon^{189}\text{Os}$ and the $\epsilon^{190}\text{Os}$ both measure the
309 same neutron capture reaction, an error-weighted average of these two yielded $\delta^{65}\text{Cu}$ values of -0.4 ± 1.0

310 (95% conf.). This value was then averaged with that from Fig. 4C to obtain $\delta^{65}\text{Cu}$ values of -0.3 ± 0.8 (95%
311 conf.). This corrected Cu isotopic composition for the IVB iron meteorites falls in the range defined by
312 other iron meteorite groups as well as chondrites (Fig. 5). Therefore, our results imply that volatile
313 depletion in IVB meteorites did not fractionate Cu isotopes by a magnitude greater than that of the range
314 in chondritic Cu isotope values. Recent measurements of nucleosynthetic anomalies in Ni (Regelous et al.,
315 2008), Mo (Burkhardt et al., 2011), Ru (Chen et al., 2010; Fischer-Gödde et al., 2015), Pd (Mayer et al.,
316 2015) and W (Qin et al., 2008; Kruijer et al., 2012; Wittig et al., 2013) isotopes show that IVB irons have
317 the largest isotopic anomalies among iron meteorites, similar to the scales observed in chondrites. The
318 IVB irons also show a chondritic pre-exposure Cu isotope composition within our current analytical
319 precision (Fig. 5).

320

321 **6. Conclusions**

322 This study presents Cu isotopic compositions for 12 of the 14 known IVB iron meteorites. IVB magmatic
323 iron meteorites show significant Cu isotopic variations ($-5.84 \text{ ‰} < \delta^{65}\text{Cu} < -0.24 \text{ ‰}$) that resulted from
324 neutron capture on ^{62}Ni induced by cosmic ray exposure. The $\delta^{65}\text{Cu}$ displays clear negative correlations
325 with $\epsilon^{192}\text{Pt}$ and $\epsilon^{190}\text{Os}$ and positive correlations with $\epsilon^{189}\text{Os}$ and $\epsilon^{182}\text{W}$, with Weaver Mountains
326 representing the least and Tlacotepec representing the most radiation-damaged samples. The $\delta^{65}\text{Cu}-\epsilon^{192}\text{Pt}$,
327 $\delta^{65}\text{Cu}-\epsilon^{190}\text{Os}$, $\delta^{65}\text{Cu}-\epsilon^{189}\text{Os}$ correlations defined by the IVB irons yield an average pre-exposure $\delta^{65}\text{Cu}$ of
328 $-0.3 \pm 0.8 \text{ ‰}$ (95% conf.), which agrees well with the Cu isotopic compositions of other iron meteorite
329 groups and falls within the range of chondrites. The pre-irradiation Cu isotope composition of IVB irons
330 ($-0.3 \pm 0.8 \text{ ‰}$) provides no support for an evaporative loss of Cu as the cause of the low Cu/Ni ratio of the
331 IVB parental liquid (Campbell and Humayun, 2005). Despite the large uncertainty of the pre-irradiation
332 $\delta^{65}\text{Cu}$ for IVBs, it is clear that the extreme volatile Cu depletion in IVB irons was not accompanied by
333 enough $\delta^{65}\text{Cu}$ variation to set it apart from other iron meteorite groups. The large neutron capture effect
334 observed in IVB irons is due to the high Ni/Cu ratios of these meteorites. Thus, this effect may not be

335 apparent in most other irons, but may affect some other irons that have undergone significant GCR
336 exposure with lower Ni/Cu ratios than IVBs.

337

338 **Acknowledgements**

339 We thank Julien Foriel for maintaining the clean lab and the MC-ICP-MS facilities at Washington
340 University in St. Louis. We thank the Smithsonian Institution (USNM), American Museum of Natural
341 History (AMNH), Naturhistorisches Museum (Wien), the Monnig Collection at Texas Christian
342 University, Arizona State University, and Harvard Mineralogical Museum are thanked for kindly
343 providing samples. This work was supported by grants from the NASA Cosmochemistry program to
344 Frédéric Moynier (NNX12AH70G) and Munir Humayun (NNX13AI06G).

345 FM thanks the European Research Council for funding under the H2020 framework program/ERC grant
346 agreement #637503 (Pristine), as well as the financial support of the UnivEarthS Labex program at
347 Sorbonne Paris Cité (ANR-10-LABX-0023 and ANR-11-IDEX-0005-02), the ANR through a chaire
348 d'excellence Sorbonne Paris Cité.

349 **References**

- 350 Albarède F. (2004) The stable isotope geochemistry of copper and zinc. in: Johnson, C.M., Beard, B.L.,
351 Albarède, F. (Eds.), *Geochemistry of Non-Traditional Stable Isotopes*, Mineralogical Soc.
352 America, Washington, pp. 409-427.
- 353 Archer C., and Vance D. (2004) Mass discrimination correction in multiple-collector plasma source mass
354 spectrometry: an example using Cu and Zn isotopes. *J. Anal. At. Spectrom.* 19, 656-665.
- 355 Barrat J.A., Zanda B., Moynier F., Bollinger C., Liorzou C. and Bayon G. (2012) Geochemistry of CI
356 chondrites: Major and trace elements, and Cu and Zn Isotopes. *Geochim. Cosmochim. Acta* 83,
357 79-92.
- 358 Ben Othman, D., Luck J.M., Bodinier J.L., Arndt N.T. and Albarede F. (2006) Cu-Zn isotopic variations
359 in the Earth's mantle (abstract). *Geochim. Cosmochim. Acta* 70, 46-46.
- 360 Bigalke M., Weyer S. and Wilcke W. (2010) Stable Copper Isotopes: A Novel Tool to Trace Copper
361 Behavior in Hydromorphic Soils. *Soil Sci. Soc. Am. J.* 74, 60-73.
- 362 Bigalke M., Weyer S. and Wilcke W. (2011) Stable Cu isotope fractionation in soils during oxic
363 weathering and podzolization. *Geochim. Cosmochim. Acta* 75, 3119-3134.
- 364 Bishop M.C., Moynier F., Weinstein C., Fraboulet J.G., Wang K. and Foriel J.(2012) The Cu isotopic
365 composition of iron meteorites. *Meteorit. Planet. Sci.* 47, 268-276.
- 366 Braxton D. and Mathur R. (2011) Exploration Applications of Copper Isotopes in the Supergene
367 Environment: A Case Study of the Bayugo Porphyry Copper-Gold Deposit, Southern Philippines.
368 *Econ. Geol.* 106, 1447-1463.
- 369 Burkhardt C., Kleine T., Oberli F., Pack A., Bourdon B. and Wieler R.(2011) Molybdenum isotope
370 anomalies in meteorites: constraints on solar nebula evolution and origin of the Earth. *Earth*
371 *Planet. Sci. Lett.* 312, 390–400.
- 372 Burkhardt C., Kleine T., Dauphas N. and Wieler R. (2012) Nucleosynthetic tungsten isotope anomalies in
373 acid leachates of the Murchison chondrite: implications for hafnium-tungsten chronometry.
374 *Astrophys. J. Lett.* 753, 6.

- 375 Campbell A.J. and Humayun M. (2005) Compositions of group IVB iron meteorites and their parent melt.
376 *Geochim. Cosmochim. Acta* 69, 4733-4744.
- 377 Campbell T. J. and Humayun M. (2012) Siderophile element abundances in the Ni-rich ataxites Gebel
378 Kamil, Dumont, and Tinnie. *Lunar Planet. Sci. Conf.* **43**, abstract #2833.
- 379 Chen J.H., Papanastassiou D.A. and Wasserburg G.J. (2010) Ruthenium endemic isotope effects in
380 chondrites and differentiated meteorites. *Geochim. Cosmochim. Acta* 74, 3851–3862.
- 381 Dauphas, N., Marty, B. and Reisberg, L. (2002) Molybdenum evidence for inherited planetary scale
382 isotope heterogeneity of the protosolar nebula. *Astrophys. J.* 565, 640-644.
- 383 Fischer-Gödde M., Burkhardt C., Kruijer T. S. and Kleine T. (2015) Ru isotope heterogeneity in the solar
384 protoplanetary disk. *Geochim. Cosmochim. Acta* **168**, 151–171.
- 385 Goldstein J.I., Scott E.R.D. and Chabot N.L. (2009) Iron meteorites: Crystallization, thermal history,
386 parent bodies, and origin. *Chemie der Erde - Geochemistry* 69, 293-325.
- 387 Herzog G.F. (2007) Cosmic-ray exposure ages of meteorites. In: Holland, H. D., Turekian, K. K.(Eds.),
388 *Treatise on Geochemistry*. Elsevier, Amsterdam, pp.1–36.
- 389 Herzog G.F., Moynier F., Albarede F. and Berezhnoy A.A. (2009) Isotopic and elemental abundances of
390 copper and zinc in lunar samples, Zagami, Pele's hairs, and a terrestrial basalt. *Geochim.*
391 *Cosmochim. Acta* 73, 5884-5904.
- 392 Huang S. and Humayun M. (2008) Osmium isotope anomalies in group IVB irons: cosmogenic or
393 nucleosynthetic contributions (abstract). *Lunar Planet Sci.* 39, #1168.
- 394 Humayun M. and Clayton R.N. (1995) Potassium isotope cosmochemistry: Genetic implications of
395 volatile element depletion, *Geochim. Cosmochim. Acta* 59, 2131-2148.
- 396 Humayun M. and Cassen P. (2000) Processes determining the volatile abundances of the meteorites and
397 terrestrial planets, In: R. M. Canup and K. Righter (eds.) *Origin of the Earth and Moon*,
398 University of Arizona Press, Tucson, pp. 3-23.
- 399 Humayun M. and Koeberl C. (2004) Potassium isotopic composition of Australian tektites. *Meteorit.*
400 *Planet. Sci.* 39, 1509–1516.

- 401 Humayun M. (2012) Chondrule cooling rates inferred from diffusive profiles in metal lumps from the
402 Acfer 097 CR2 chondrite. *Meteoritics Planet. Sci.* **47**, 1191-1208.
- 403 Kleine T., Munker C., Mezger K., and Palme H. (2002) Rapid accretion and early core formation on
404 asteroids and the terrestrial planets from Hf-W chronometry. *Nature* 418, 952–955.
- 405 Kleine T., Mezger K., Munker C., Palme H. and Bischoff A. (2004) ^{182}Hf - ^{182}W isotope systematics of
406 chondrites, eucrites, and martian meteorites: Chronology of core formation and early mantle
407 differentiation in Vesta and Mars. *Geochim. Cosmochim. Acta* 68, 2935-2946.
- 408 Kleine T., Mezger K., Palme H., Scherer E. and Munker C. (2005) Early core formation in asteroids and
409 late accretion of chondrite parent bodies: Evidence from ^{182}Hf - ^{182}W in CAIs, metal-rich
410 chondrites, and iron meteorites. *Geochim. Cosmochim. Acta* 69, 5805-5818.
- 411 Kruijer T.S., Sprung P., Kleine T., Leya I., Burkhardt C. and Wieler R., (2012) Hf–W chronometry of
412 core formation in planetesimals inferred from weakly irradiated iron meteorites. *Geochim.*
413 *Cosmochim. Acta* 99, 287-304
- 414 Kruijer T.S., Fischer-Godde M., Kleine T., Sprung P., Leya I. and Wieler R. (2013) Neutron capture on Pt
415 isotopes in iron meteorites and the Hf-W chronology of core formation in planetesimals. *Earth*
416 *Planet. Sci. Lett.* 361, 162-172.
- 417 Kruijer T. S., Touboul M., Fischer-Gödde M., Bermingham K. R., Walker R. J. and Kleine T. (2014)
418 Protracted core-formation and rapid accretion of protoplanets. *Science* **344**, 1150-1154.
- 419 Lee D. C. (2005) Protracted core formation in asteroids: Evidence from high precision W isotopic data.
420 *Earth Planet. Sci. Lett.* 237, 21-32.
- 421 Lee T., Papanastassiou D.A. and Wasserburg, G.J. (1976) Demonstration of ^{26}Mg excess in Allende and
422 evidence for ^{26}Al . *Geophys. Res. Lett* 3, 109-112.
- 423 Leya I., Wieler R. and Halliday A.N. (2003) The influence of cosmic-ray production on extinct nuclide
424 systems. *Geochim. Cosmochim. Acta* 67, 529-541.
- 425 Leya I. and Masarik J. (2013) Thermal neutron capture effects in radioactive and stable nuclide systems.
426 *Meteoritics Planet. Sci.* **48**, 665–685.

- 427 Li W., Jackson S.E., Pearson N.J., Alard O. and Chappell B.W. (2009) The Cu isotopic signature of
428 granites from the Lachlan Fold Belt, SE Australia. *Chem. Geol.* 258, 38-49.
- 429 Lodders K. (2003) Solar system abundances and condensation temperatures of the elements. *Astrophys. J.*
430 591, 1220-1247.
- 431 Luck J.M., Ben Othman D., Barrat J.A. and Albarede F. (2003) Coupled ^{63}Cu and ^{16}O excesses in
432 chondrites. *Geochim. Cosmochim. Acta* 67, 143-151.
- 433 Luck J.M., Othman D.B. and Albarède F. (2005) Zn and Cu isotopic variations in chondrites and iron
434 meteorites: Early solar nebula reservoirs and parent-body processes. *Geochim. Cosmochim. Acta*
435 69, 5351-5363.
- 436 Ludwig K.R. (2003) *Isoplot 3.00: a Geochronological Toolkit for Microsoft Excel*. Berkeley
437 Geochronology Center Special Publication vol. 4, p. 70.
- 438 **Lugmair G.W. and Shukolyukov A. (1998) Early solar system timescales according to ^{53}Mn - ^{53}Cr
439 systematics. *Geochim. Cosmochim. Acta* 62, 2863-2886.**
- 440 Marechal C.N., Telouk P. and Albarede F. (1999) Precise analysis of copper and zinc isotopic
441 compositions by plasma-source mass spectrometry. *Chem. Geol.* 156, 251-273.
- 442 Markowski A., Quitte G., Halliday A.N. and Kleine T. (2006a) Tungsten isotopic compositions of iron
443 meteorites: Chronological constraints vs. cosmogenic effects. *Earth Planet. Sci. Lett.* 242, 1-15.
- 444 Markowski A., Leya I., Quitte G., Ammon K., Halliday A.N. and Wieler R. (2006b) Correlated helium-3
445 and tungsten isotopes in iron meteorites: Quantitative cosmogenic corrections and planetesimal
446 formation times. *Earth Planet. Sci. Lett.* 250, 104-115.
- 447 Masarik J. (1997) Contribution of neutron-capture reactions to observed tungsten isotopic ratios. *Earth*
448 *Planet. Sci. Lett.* 152: 181-185.
- 449 Mayer B., Wittig N., Humayun M. and Leya I. (2015) Palladium isotopic evidence for nucleosynthetic
450 and cosmogenic isotope anomalies in IVB iron meteorites. *Astrophys. Jour.* **108**, 180 (8 pp).
- 451 Moynier F., Albarede F. and Herzog G.F. (2006) Isotopic composition of zinc, copper, and iron in lunar
452 samples. *Geochim. Cosmochim. Acta* 70, 6103-6117.

453 Moynier F., Blichert-Toft J., Telouk P., Luck J.M. and Albarede F. (2007) Comparative stable isotope
454 geochemistry of Ni, Cu, Zn, and Fe in chondrites and iron meteorites. *Geochim. Cosmochim.*
455 *Acta* 71, 4365-4379.

456 Moynier F., Yin QZ, Irisawa K., Boyet M., Jacobsen B. and Rosing M. (2010a) A coupled ^{182}W - ^{142}Nd
457 constraint for early Earth differentiation. *Proc. Natl. Acad. Sci. U.S.A.* 107, 10810-10814.

458 Moynier F., Koeberl C., Beck P., Jourdan F. and Telouk P. (2010b) Isotopic fractionation of Cu in tektites.
459 *Geochim. Cosmochim. Acta* 74, 799-807.

460 Mughabghab S.F. (2003) The thermal neutron capture cross sections resonance integrals and G-factors.
461 International Atomic Energy Agency (International Nuclear Data Committee), pp. 1–31.

462 Qin L.P., Dauphas N., Wadhwa M., Masarik J. and Janney P.E. (2008) Rapid accretion and differentiation
463 of iron meteorite parent bodies inferred from ^{182}Hf - ^{182}W chronometry and thermal modeling.
464 *Earth Planet. Sci. Lett.* 273, 94-104

465 Rasmussen K.L., Malvin D.J., Buchwald V.F. and Wasson J.T. (1984) Compositional trends and cooling
466 rates of group-IVB iron meteorites. *Geochim. Cosmochim. Acta* 48, 805-813.

467 Regelous M., Elliott T. and Coath C.D. (2008) Nickel isotope heterogeneity in the early Solar System.
468 *Earth Planet. Sci. Lett.* 272, 330-338.

469 Righter K., Pando K.M., Danielson L. and Lee C.T. (2010) Partitioning of Mo, P and other siderophile
470 elements (Cu, Ga, Sn, Ni, Co, Cr, Mn, V, and W) between metal and silicate melt as a function of
471 temperature and silicate melt composition. *Earth Planet. Sci. Lett.* 291, 1-9.

472 Savage P., Moynier F., Chen H., Siebert J., Badro J., Puchtel I., and Shofner G. (2015) Copper isotope
473 evidence for large-scale sulphide fractionation during Earth's differentiation. *Geochem. Perspect.*
474 *Lett.* 1, 53-64

475 Schersten A., Elliott T., Hawkesworth C., Russell S. and Masarik J. (2006) Hf-W evidence for rapid
476 differentiation of iron meteorite parent bodies. *Earth Planet. Sci. Lett.* 241, 530-542.

477 Schoenberg R., Kamber B. S., Collerson K. D., and Eugster O. (2002) New W-isotope evidence for rapid
478 terrestrial accretion and very early core formation. *Geochim. Cosmochim. Acta* 66, 3151–3160.

479 Scott E.R.D. (1972) Chemical fractionation in iron meteorites and its interpretation. *Geochim.*
480 *Cosmochim. Acta* 36, 1205-1236.

481 Scott E.R.D. (1978) Iron meteorites with low Ga and Ge concentrations-composition, structure and
482 genetic relationships. *Geochim. Cosmochim. Acta* 42, 1243-1251.

483 Trinquier, A., Birck, J.L. and Allegre, C.J. (2007) Widespread ^{54}Cr heterogeneity in the inner solar system.
484 *Astrophys. J.* 655, 1179-1185.

485 Vockenhuber C., Oberli F., Bichler M., Ahmad I., Quitte G., Meier M., Halliday A.N., Lee D.C.,
486 Kutschera W., Steier P., Gehrke R.J. and Helmer R.G. (2004) New half-life measurement of ^{182}Hf :
487 Improved chronometer for the early solar system. *Phys. Rev. Lett.* 93, 4.

488 Voshage H. and Feldmann H. (1979) Investigations on cosmic-ray-produced nuclides in iron meteorites, 3.
489 Exposure ages, meteoroid sizes and sample depths determined by mass spectrometric analyses of
490 potassium and rare gases. *Earth Planet. Sci. Lett.* 45, 293-308.

491 Voshage H. (1984) Investigations of cosmic-ray-produced nuclides in iron meteorites, 6. The Signer-Nier
492 model and the history of the cosmic radiation. *Earth Planet. Sci. Lett.* 71, 181-194.

493 Walker R.J., McDonough W.F., Honesto J., Chabot N.L., McCoy T.J., Ash R.D. and Bellucci J.J. (2008)
494 Modeling fractional crystallization of group IVB iron meteorites. *Geochim. Cosmochim. Acta* 72,
495 2198-2216.

496 Walker R.J. (2012) Evidence for homogeneous distribution of osmium in the protosolar nebula. *Earth*
497 *Planet. Sci. Lett.* 351-352, 36-44.

498 Weinstein C., Moynier F., Wang K., Paniello R., Foriel J., Catalano J. and Pichat S. (2011) Isotopic
499 fractionation of Cu in plants. *Chem. Geol.* 286, 266-271.

500 Williams J.T. and Humayun M. (2013) Origin of the IVB irons in a hit-and-run collision (abstract). *Lunar*
501 *Planet Sci.* 44, #2784.

502 Wittig N., Humayun M., Brandon A.D., Huang S. and Leya I. (2013) Coupled W-Os-Pt isotope
503 systematics in IVB iron meteorites: In situ neutron dosimetry for W isotope chronology. *Earth*
504 *Planet. Sci. Lett.* 361, 152-161.

- 505 Yang J.J., Goldstein J.I., Michael J.R., Kotula P.G. and Scott E.R.D. (2010) Thermal history and origin of
506 the IVB iron meteorites and their parent body. *Geochim. Cosmochim. Acta* 74, 4493-4506.
- 507 Yin Q.Z., Jacobsen S.B., Yamashita K., Blichert-Toft J., Telouk P. and Albarede F. (2002) A short
508 timescale for terrestrial planet formation from Hf-W chronometry of meteorites. *Nature* 418, 949-
509 952.

Figure Captions

Fig.1. $\delta^{65}\text{Cu}$ range for the bulk Silicate Earth (BSE), tektites, lunar basalts and soils, chondrites, IVB and other group iron meteorites. The dashed line represents the average Cu isotopic composition of BSE: $\delta^{65}\text{Cu} = 0.07 \pm 0.10 \text{ ‰}$ (2 s.d.; Savage et al., 2015). tektite data are from Moynier et al. (2010b); Lunar soil and basalt data are from Moynier et al. (2006) and Herzog et al. (2009); chondrite data are from Luck et al. (2003) and Barrat et al. (2012); and iron meteorite data are from Bishop et al. (2012). The IVB iron data (before cosmogenic neutron capture corrections) are from this study.

Fig.2. $\delta^{65}\text{Cu}$ versus the degree of crystal-liquid differentiation as represented by the Re concentration for IVB iron meteorites. The external uncertainty is ± 0.10 (2 s.d.) for $\delta^{65}\text{Cu}$. Re data are from Walker et al. (2008), except for Dumont which were determined by Campbell and Humayun (2012).

Fig.3. $\delta^{65}\text{Cu}$ versus the Ni/Cu ratio of IVB iron meteorites. The five red dashed lines represent modeled ^{63}Ni - ^{63}Cu evolution diagrams (isochron lines), which assume the initial $^{63}\text{Ni}/^{60}\text{Ni}$ of 1×10^{-5} and $\delta^{65}\text{Cu}$ of 0. The differences in the slopes of the four correlation lines correspond to the differences in times of crystallization.

Fig.4. Correlation of $\delta^{65}\text{Cu}$ (this study) with GCR-modified isotopes (Wittig et al., 2013) (A) $\varepsilon^{189}\text{Os}$, (B) $\varepsilon^{190}\text{Os}$, and (C) $\varepsilon^{192}\text{Pt}$ in IVB iron meteorites. In each panel, the dashed line represents the best-fit linear regression line calculated using Isoplot (Ludwig, 2003) and projection to the x-axis intercept of 0 yields the pre-GCR irradiation $\delta^{65}\text{Cu}$ of the IVB iron meteorite group (black bar, 2 s.d.). Error bars on symbols represent the uncertainties (see Table 2). Uncertainty of $\delta^{65}\text{Cu}$ is 0.10‰, which is not resolvable in this figure set due to large span of Cu variation.

Fig.5. Comparison of Cu isotopic composition between primitive meteorites and pre-exposure IVB iron meteorites. The yellow band represents the $\delta^{65}\text{Cu}$ value of Bulk Silicate Earth, i.e. $0.07 \pm 0.10 \text{ ‰}$ (2 s.d.; Savage et al., 2015). Carbonaceous and ordinary chondrites data are from Luck et al. (2003) and Barrat et al. (2012).

Table 1. Copper isotopic compositions of USGS geostandards.

Geostandard	$\delta^{65}\text{Cu}$	2s.d.	Reference
BCR-1	0.21	0.09	This study
	0.07	0.08	Archer and Vance (2004)
BCR-2	0.20	0.09	This study
	0.22	0.08	Bigalke et al., (2010)
	0.18	0.08	Bigalke et al., (2011)
BIR-1	0.04	0.09	This study
	-0.02	0.10	Li et al., (2009)
BHVO-2	0.13	0.09	This study
	0.10	0.07	Moynier et al., (2010b)
AGV-2	-0.02	0.09	This study
	0.10	0.11	Moynier et al., (2010b)
PCC-1	0.17	0.09	This study
DTS-1	0.08	0.09	This study

Table 2. Cu, W, Os, and Pt isotope data of IVB iron meteorites

	$\delta^{65}\text{Cu}^{\text{a}}$	n^{b}	Ni (wt.%)	Cu (ppm)	Ni/Cu (10^4)	Re (ppm) ^c	$\epsilon^{182}\text{W}^{\text{d}}$	2se_m	$\epsilon^{189}\text{Os}^{\text{d}}$	2se_m^{e}	$\epsilon^{190}\text{Os}^{\text{d}}$	2se_m	$\epsilon^{192}\text{Pt}^{\text{d}}$	2s.d.^{f}
Cape of Good														
Hope	-2.40	2	15.68	1.30	12.0	3.06	-3.6	0.18	-0.32	0.11	0.11	0.06	24.6	0.8
Dumont	-4.53	2	16.30 ^g	1.27	12.9	2.63 ^g	-3.85	0.06	-0.23	0.07	0.26	0.01	23.6	0.3
Hoba	-1.53	3	16.43	1.31	12.6	2.43	-3.61	0.09	-0.06	0.03	0.00	0.00	13.7	0.4
Iquique	-1.96	2	15.99	1.39	11.5	3.21	-3.55	0.03	-0.25	0.05	0.18	0.03	24.3	1.0
Kokomo	-4.30	2	16.29	1.27	12.9	3.15	-3.55	0.12	-0.25	0.06	0.15	0.03	31.8	0.8
Santa Clara	-2.26	3	17.64	1.68	10.5	1.81	-3.64	0.06	-0.34	0.01	0.14	0.10	13.8	0.4
Skookum	-3.47	3	17.83	1.63	11.0	1.37	-3.59	0.17	-0.16	0.00	0.19	0.03	6.3	0.6
Tawallah Valley	-2.89	2	17.66	1.77	10.0	1.37	-3.72	0.17	-0.24	0.10	0.06	0.05	8.6	0.5
Tinnie	-1.54	2	17.69	1.79	9.9	1.53	-3.57	0.07	-0.05	0.03	0.03	0.02	6.3	0.3
Tlacotepec	-5.84	3	16.06	1.26	12.7	3.10	-4.21	0.13	-0.64	0.06	0.39	0.07	52.8	0.4
Weaver Mountains	-0.24	3	17.87	1.65	10.9	1.40	-3.33	0.12	-0.03	0.01	0.06	0.03	4.4	0.3
Warburton Range	-2.42	2	17.84	1.77	10.1	1.23	-3.42	0.16	0.02	0.06	0.05	0.08	5.9	0.5

^a External reproducibilities (2 s.d.) are estimated to be ± 0.10 ‰ for $\delta^{65}\text{Cu}$

^b n=number of repeat measurements by MC-ICP-MS

^c Re data for IVB iron meteorites from Walker et al. (2008)

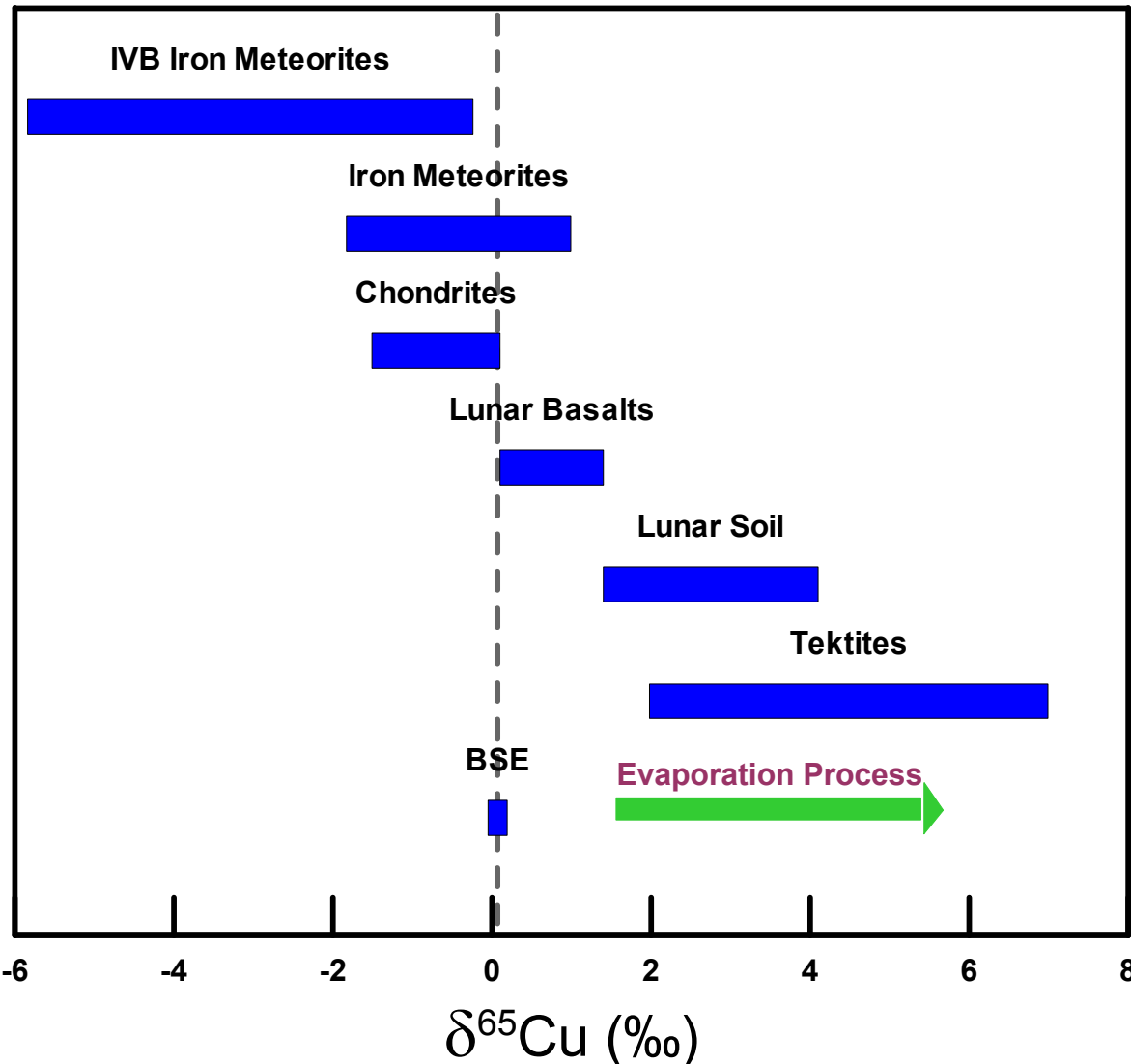
^d $\epsilon^{182}\text{W}$, $\epsilon^{189}\text{Os}$, $\epsilon^{190}\text{Os}$, and $\epsilon^{192}\text{Pt}$ data from Wittig et al. (2013)

^e Uncertainties of W and Os isotope data are given as standard error of the mean (2se_m) derived from replicate measurements of the same digestions

^f Uncertainties of Pt isotopes are given as in-run standard deviation (2s.d.)

^g data from Campbell and Humayun (2012)

Figure 1



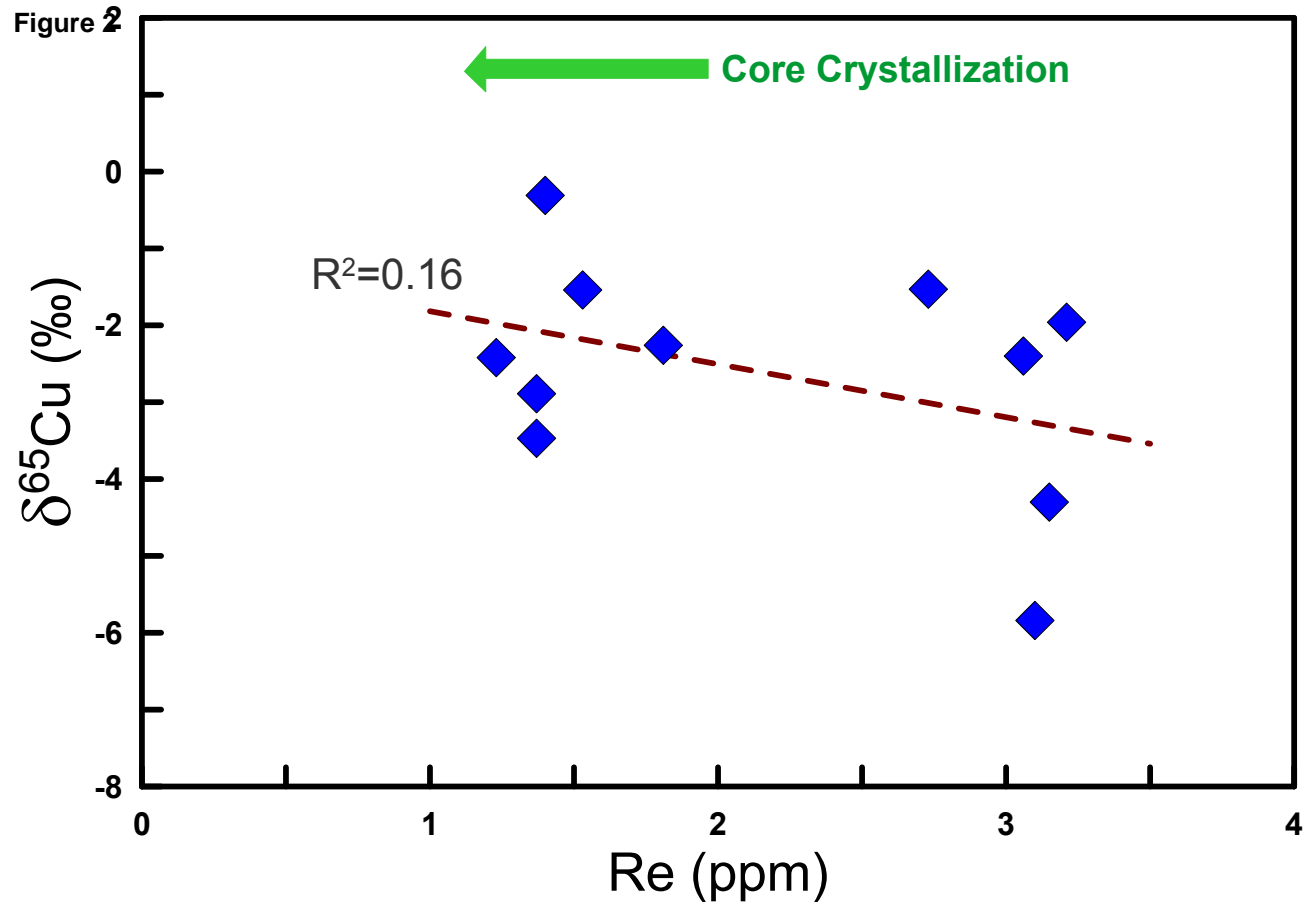
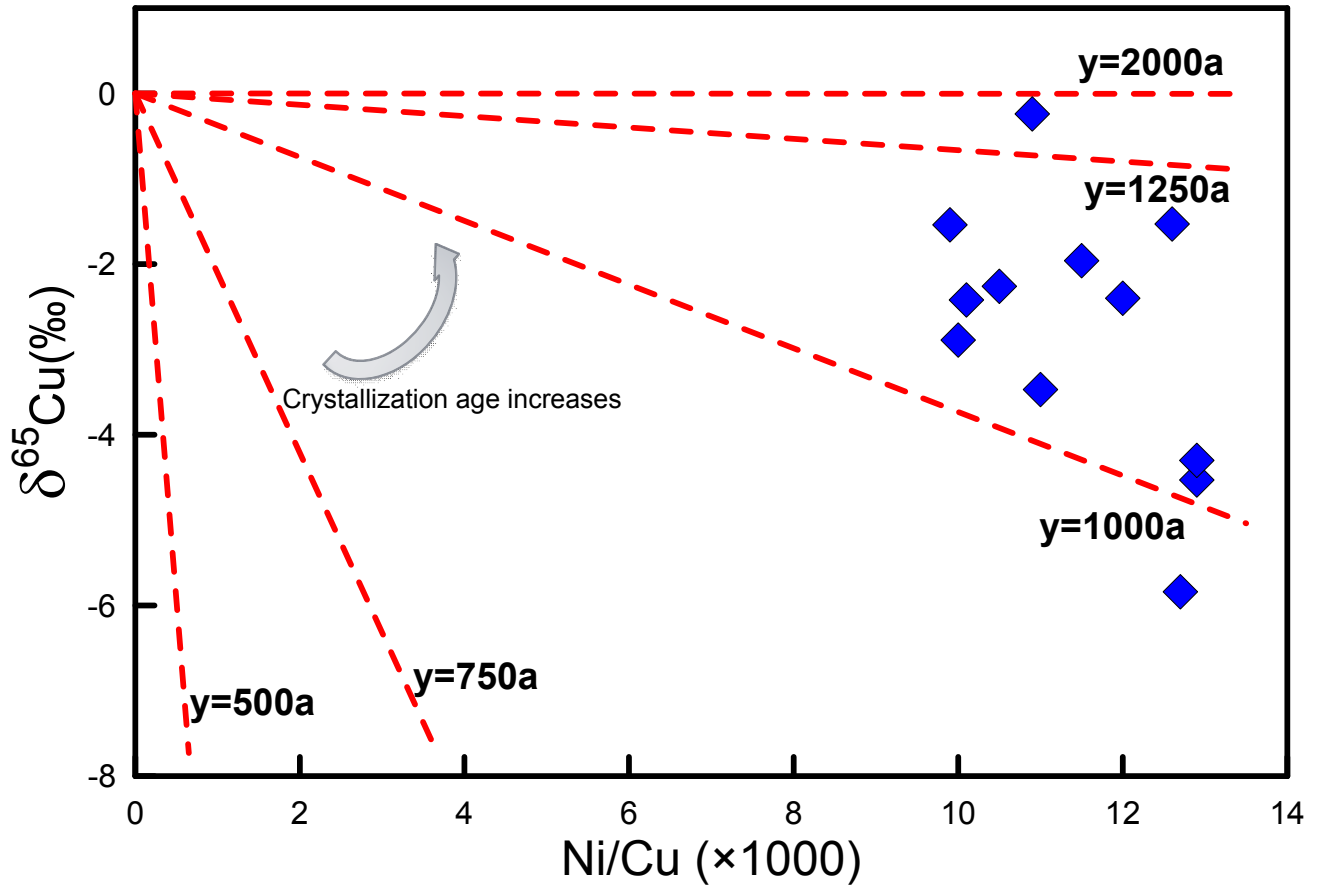


Figure 3



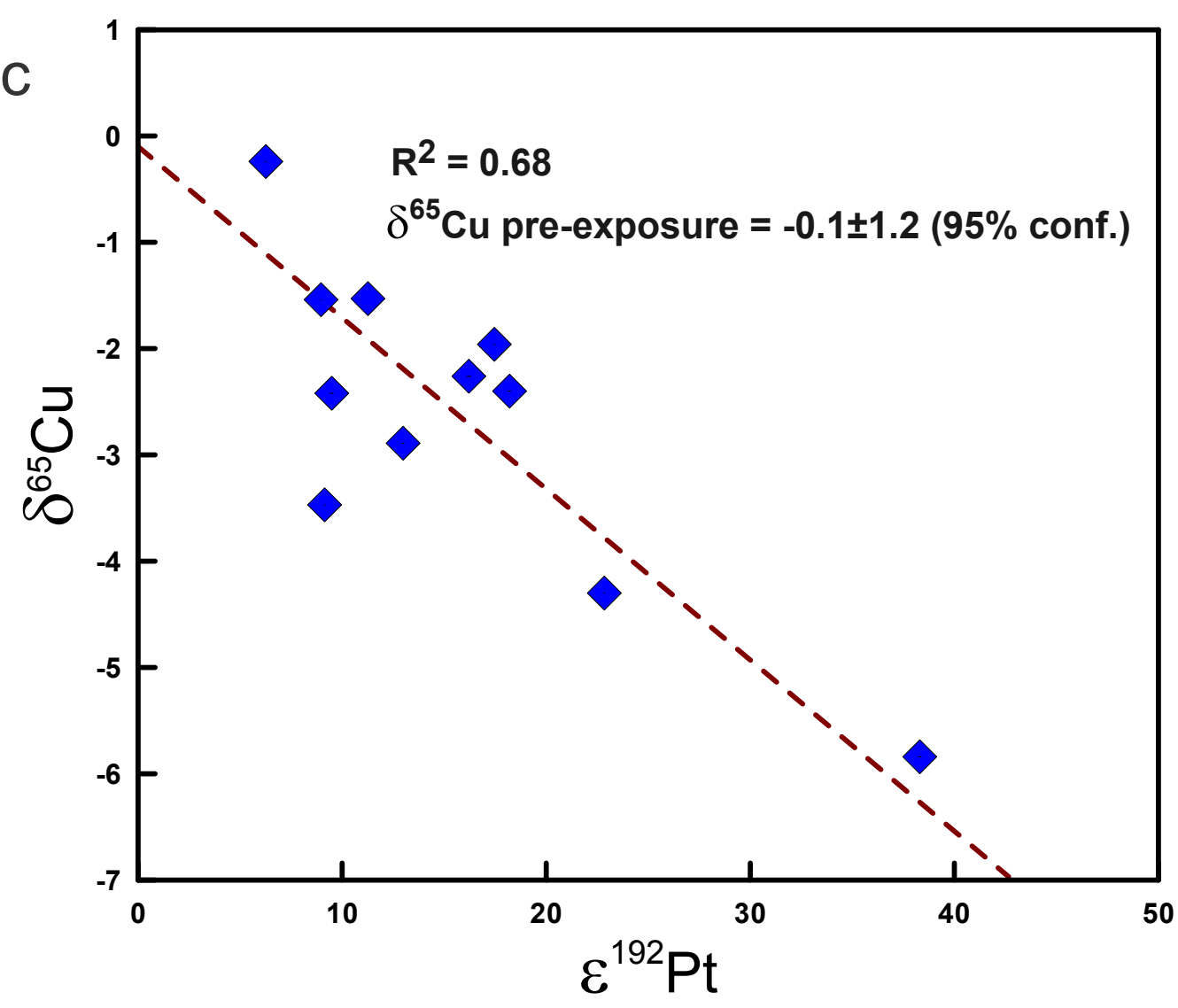
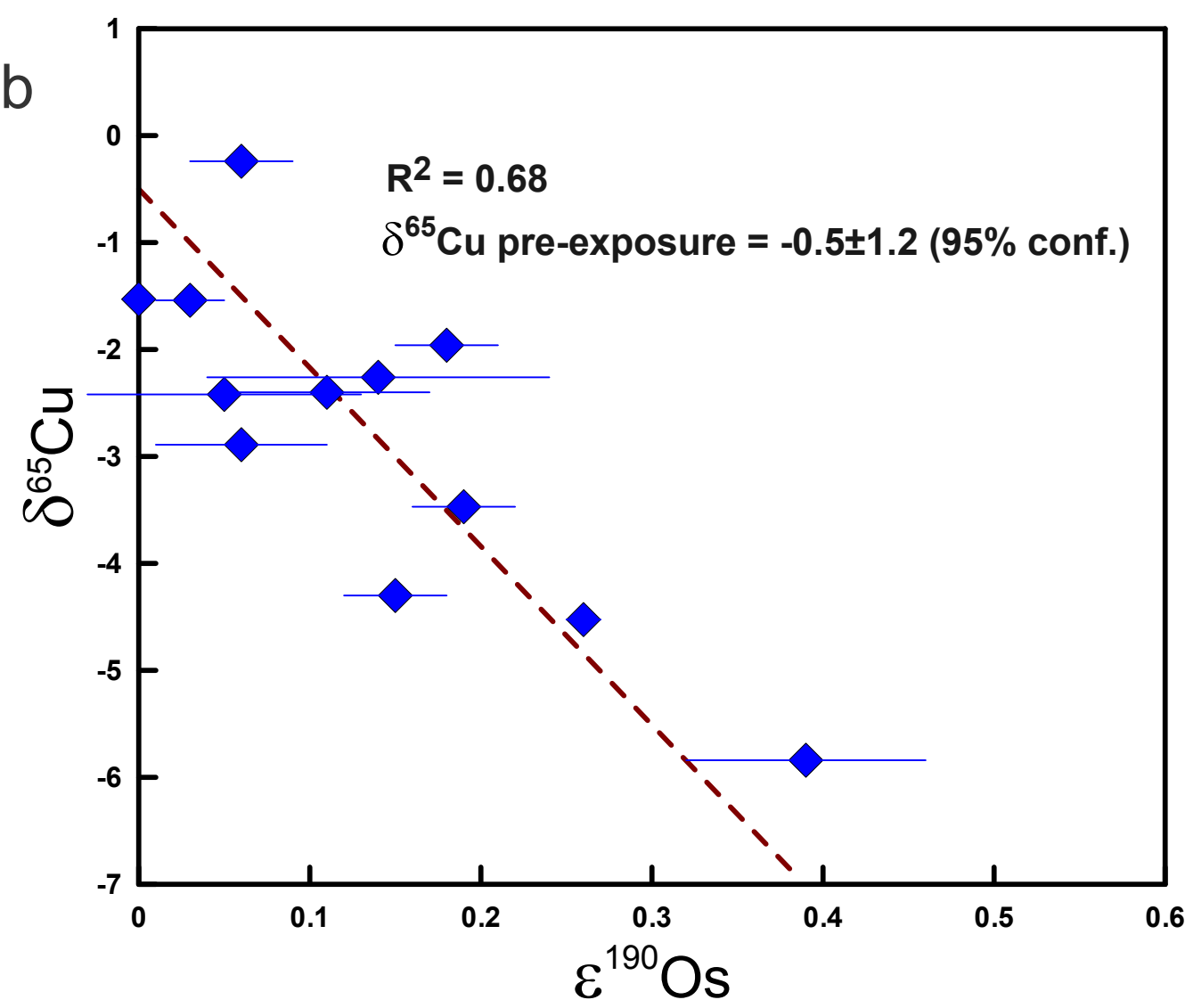
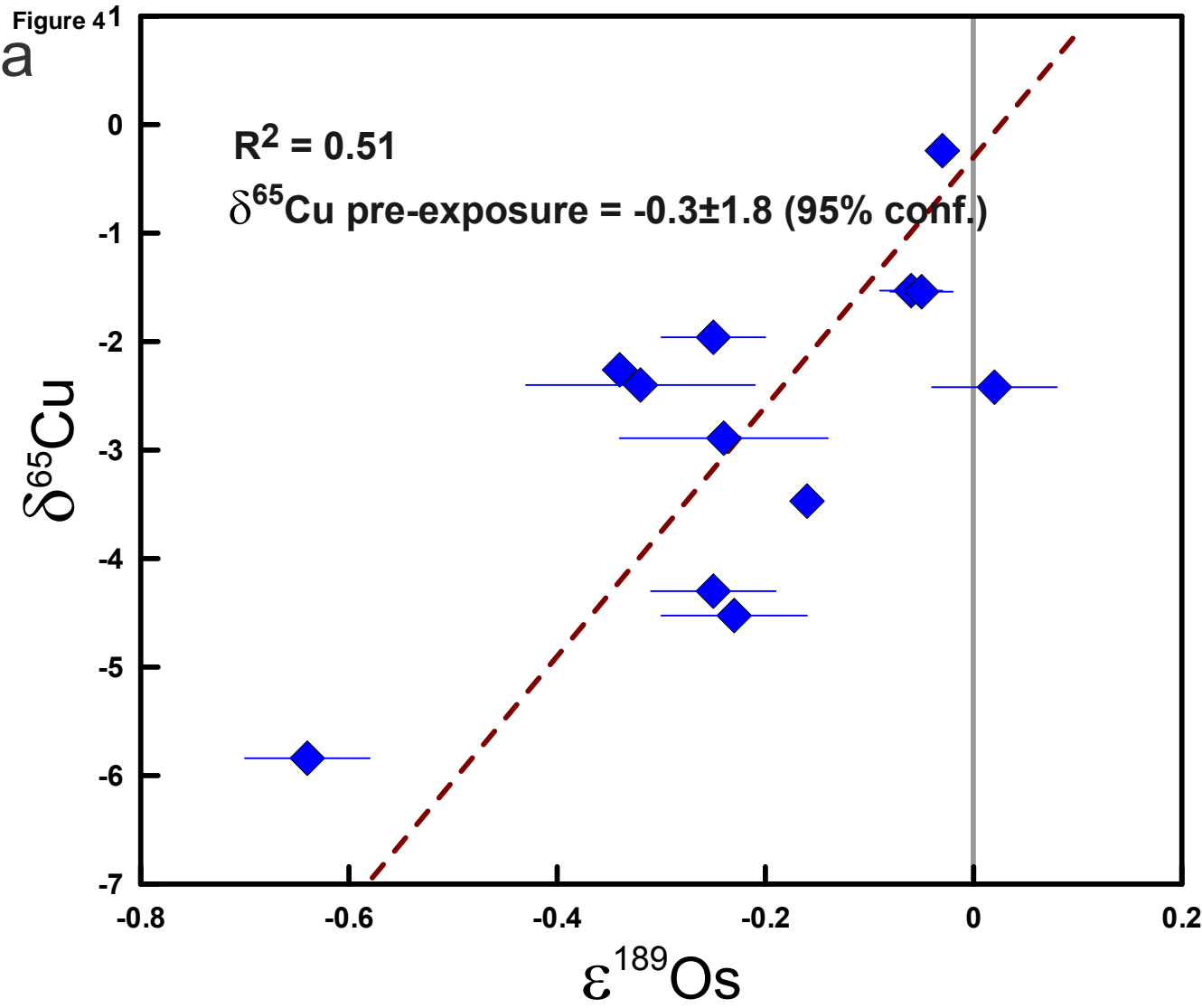


Figure 5

